Over 40 cd/A Efficient Green Quantum Dot Electroluminescent Device Comprising Uniquely Large-Sized Quantum Dots

Ki-Heon Lee,[†] Jeong-Hoon Lee,[†] Hee-Don Kang,[†] Byoungnam Park,[†] Yongwoo Kwon,[†] Heejoo Ko,[‡] Changho Lee,[‡] Jonghyuk Lee,[‡] and Heesun Yang[†,*]

[†]Department of Materials Science and Engineering, Hongik University, Seoul 121-791, Korea and [‡]Display Research Center, Samsung Display Co., Ltd. Yongin, Kyunggi-do 446-811, Korea

ABSTRACT Green CdSe@ZnS quantum dots (QDs) of 9.5 nm size with a composition gradient shell are first prepared by a single-step synthetic approach, and then 12.7 nm CdSe@ZnS/ZnS QDs, the largest among ZnS-shelled visible-emitting QDs available to date, are obtained through the overcoating of an additional 1.6 nm thick ZnS shell. Two QDs of CdSe@ZnS and CdSe@ZnS/ZnS are incorporated into the solution-processed hybrid QD-based light-emitting diode (QLED) structure, where the QD emissive layer (EML) is sandwiched by poly (9-vinylcarbazole) and ZnO nanoparticles as hole and electron-transport layers, respectively. We find that the presence of an additional ZnS shell makes a profound impact on device performances such as luminance and efficiencies. Compared to CdSe@ZnS QD-based devices the efficiencies of CdSe@ZnS/ZnS QD-based devices are overwhelmingly higher, specifically showing unprecedented values of peak current efficiency of 46.4 cd/A and external quantum efficiency of 12.6%. Such excellent results are likely attributable to a unique structure in CdSe@ZnS/ZnS QDs with a relatively thick ZnS outer shell as well as a well-positioned intermediate alloyed shell, enabling the effective suppression of nonradiative energy transfer between closely packed EML QDs and Auger recombination at charged QDs.

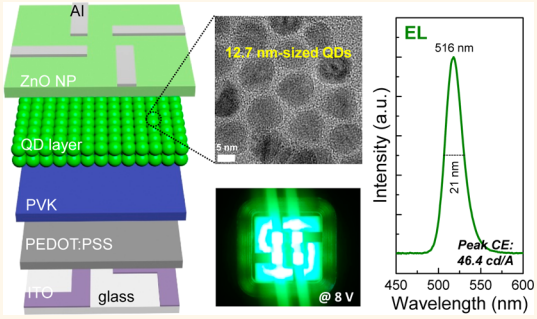

KEYWORDS: quantum dots · electroluminescence · current efficiency

Fluorescent semiconductor quantum dots (QDs) have shown great promise as visible emitters for the fabrication of electroluminescent (EL) QD-based light-emitting diodes (QLEDs). Enabled by the exceptionally color-pure emission of well-synthesized Cd-based II–VI QDs, QLEDs possess a superior color gamut property compared to state-of-the-art organic LEDs (OLEDs). To catch up with the performance level, in particular, device efficiency, of technology-mature OLEDs, significant efforts have been dedicated to improving QLED efficiency mainly by searching new types of charge-transport layers (CTLs) and/or altering the conventional device architecture.[1−19] In a prototypical QLED structure, the QD emitting layer (EML) of multiple monolayers (MLs) comes into direct contact with two CTLs of hole transport layer (HTL) and electron transport layer (ETL) for the efficient injection of charge carriers to the active QD region from the respective electrodes. Among the combinations of HTL/ETL, hybrid devices with organic HTL (*e.g.*, poly(*N*,*N*′-bis-(4-butylphenyl)-*N*,*N*′-bis(phenyl)benzidine) (poly-TPD), poly[(9,9-dioctylfluorenyl-2,7-diyl)-*co*-(4,4′-(*N*-(4-*sec*-butylphenyl))diphenylamine) (TFB), poly(9-vinylcarbazole) (PVK)), and inorganic metal oxide ETL (*e.g.*, ZnO, TiO_2)[1−9] have recently gained a significant attention since in terms of efficiency and luminance they outperformed the devices comprising either organic or inorganic CTLs.[10−17] For example, in 2011, Kim *et al.* reported red (R), green (G), and blue (B) hybrid QLEDs consisting of a transfer-printed QD layer with a HTL of TFB and an ETL of sol–gel-derived TiO_2, showing peak luminances of 16380, 6425, and 423 cd/m^2,

* Address correspondence to hyang@hongik.ac.kr.

Received for review February 11, 2014 and accepted April 23, 2014.

Published online April 23, 2014
10.1021/nn500852g

respectively, and peak power efficiency (PE) of 4.25 lm/W from R-QLED.[3] Later, Holloway *et al.* demonstrated fully solution-processed, higher performance R-, G-, B-devices with peak luminances of 31000, 68000, and 4200 cd/m^2 and peak current efficiencies (CEs) of 3.9, 7.5, and 0.32 cd/A, respectively, by introducing a ZnO nanoparticle (NP) ETL with an HTL of poly-TPD.[4] Since then, ZnO NP has become the most popular ETL material for QLED fabrication. Highly bright, efficient hybrid QLEDs have been further demonstrated by employing an inverted device architecture. In those devices, ZnO NP ETL and QD EML were successively spin-deposited on an indium tin oxide (ITO) cathode, and then 4,4′-bis(carbazole-9-yl)biphenyl (CBP) HTL, MoO_3 hole injection layer (HIL), and Al anode were sequentially thermally evaporated. The completed R-, G-, B-QLEDs displayed peak luminances of 23040, 218000, and 2250 cd/m^2 along with the peak CEs of 5.7, 19.2, and 0.4 cd/A, respectively.[18] A year later, Mashford *et al.* reported R-QLEDs with a similar inverted structure but different HTL/HIL materials, and the record maximum values of a CE of 19 cd/A and an external quantum efficiency (EQE) of 18% were achieved simply through optimizing the QD EML thickness.[19] However, all inverted structure QLEDs reported to date cannot be fully solution-processed, since the solution processing of organic HTL following QD deposition would cause a destructive interlayer mixing.

The device efficiency of QLED is substantially limited by efficient nonradiative processes of inter-QD Förster resonant energy transfer (FRET) between a closely packed QD ensemble and multicarrier Auger recombination (AR) of charged QDs,[20] the degrees of which are sensitively dependent on QD structure. Hence, persistent synthetic refinements toward QD structure rendering the above nonradiative events minimized, specifically by engineering size (or shell thickness) and/or core/shell interface,[6,8,20−22] have been made for the improvement of QLED efficiency. The luminance and EQE of QLED with giant-shell CdSe/CdS QDs with shells thicker than 10 MLs were found to be 1 order of magnitude higher than those of the thin-shell QD device, even though the solution photoluminescence quantum yield (PL QY) of thin-shell QDs was much higher than that of giant-shell ones.[20] This was attributed to the suppression of both FRET and AR processes in such large-sized QDs. Another powerful strategy for minimizing AR is to insert an intermediate alloyed layer at core/shell interface, affording a smooth confinement potential.[23,24] Bae *et al.* utilized two red-emitting CdSe/CdS and CdSe/$CdSe_{0.5}S_{0.5}$/CdS QDs with similar photophysical properties and the same size (∼14 nm) for QLED fabrication and found a beneficial effect of the interfacial alloyed layer (*i.e.*, ∼1.5 nm thick $CdSe_{0.5}S_{0.5}$) on QLED efficiency as a result of the reduction of Auger decay rate.[21] Also, very recently, our group demonstrated a high-efficiency blue QLED with the peak values of a CE of 2.2 cd/A and an EQE of 7.1% by employing newly developed ternary blue (452 nm) CdZnS/ZnS QDs comprising an alloyed core/shell interface and thick shell.[8]

Herein, green-emitting, chemical composition gradient-shell CdSe@ZnS QDs are first synthesized, and then thicker shell CdSe@ZnS/ZnS QDs consisting of an additional 1.6 nm thick ZnS shell, leading to an uniquely large size of 12.7 nm, are consecutively prepared. The fluorescent stability behaviors of individual QDs against a repeated cycle of purification and ligand exchange are compared. Even though the inverted structure QLED has been claimed to be superior with respect to luminance and efficiency to the conventional counterpart, *i.e.*, ITO anode and Al cathode,[18,21] our study rather sticks to the latter to fulfill the fabrication of all solution-processed hybrid QLED consisting of poly(9-vinlycarbazole) (PVK) HTL and ZnO NP ETL. Two QLEDs integrated with CdSe@ZnS *versus* CdSe@ZnS/ZnS QDs are fabricated and their EL characteristics are compared, resulting in drastic differences in luminance and efficiencies and thus implying the crucial impact of the presence of an additional ZnS shell on device performance. Highly color-saturated green CdSe@ZnS/ZnS QD-based device displays the unprecedentedly high peak efficiencies of a CE of 46.4 cd/A and an EQE of 12.6%, whose values are more than 2 times higher compared to the best G-QLED reported earlier.[18]

RESULTS AND DISCUSSION

Composition gradient-shell CdSe@ZnS QDs have been synthesized *via* a single-step method with an appreciably modified version from the protocol in the literature[13,25] (see the Experimental Section for synthetic details). Co-injection of (S+Se)-trioctylphosphine (TOP) to a mixture of $Cd(acet)_2$ plus ZnO in oleic acid (OA) at an elevated temperature (310 °C) successfully led to the spontaneous formation of CdSe-rich core @ZnS-rich shell structure with a radially smooth composition gradient, enabled by the higher reactivity and consequent faster consumption of $Cd(OA)_2$ and Se-TOP relative to $Zn(OA)_2$ and S-TOP in the QD growth reaction.[5,25] The emission wavelength of CdSe@ZnS QDs can be readily tuned to either the blue or red side through changing the relative molar ratios of Cd/Zn and/or Se/S. Instead, in this work, the fine tailoring of emission wavelength was achievable with the constant molar ratios in both cationic and anionic precursors but with the minute variation of the injected amount of anionic mixture of (Se+S)-TOP. Normalized PL spectra of CdSe@ZnS QDs synthesized by injecting different (Se+S)-TOP amounts of 1.9−2.1 mL are shown in Figure 1a, where a systematic blue-shift is observed with increasing the anion amount, specifically from 524 to 510 nm for 1.9 and 2.1 mL of (Se+S)-TOP,

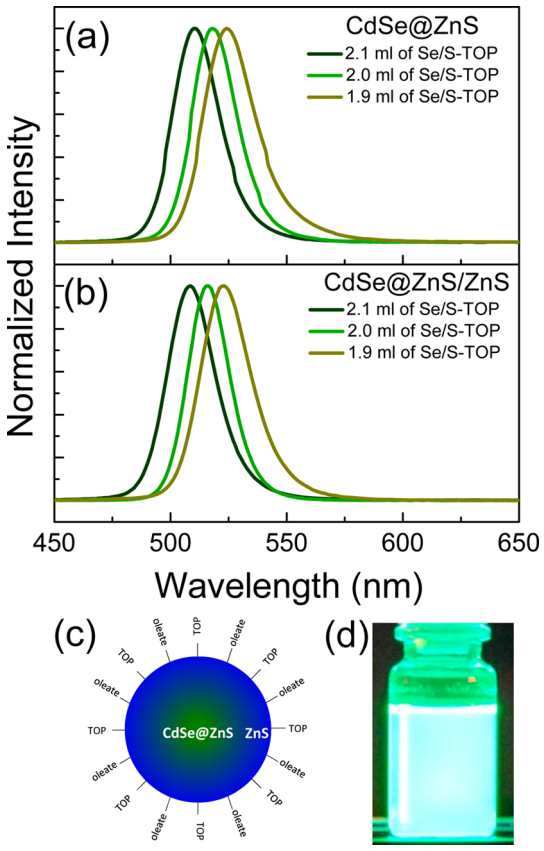

Figure 1. Normalized PL spectra of (a) CdSe@ZnS and (b) CdSe@ZnS/ZnS QDs systematically emission-tuned by slightly varying the injected amount (1.9−2.1 mL) of anionic mixture of (Se+S)-TOP. (c) Schematic illustration of CdSe@ZnS/ZnS QD sequentially comprising composition gradient-shell and additional ZnS outer shell. (d) Photographic image of strongly fluorescent (516 nm) CdSe@ZnS/ZnS QD dispersion under UV irradiation.

respectively. This result may be correlated to anion amount-dependent QD nucleation frequency.[26,27] That is, the introduction of a larger anion quantity would allow a more frequent nucleation and thus produce a larger number of QD nuclei, by which the QD growth is more limited and the relatively smaller QDs are obtained. PL QYs of a series of CdSe@ZnS were similar in the range of 40−42%. The respective CdSe@ZnS QDs were consecutively overcoated with an additional ZnS shell, producing thicker-shell CdSe@ZnS/ZnS QDs (Figure 1c). The emission wavelengths of the resulting QDs, peaking at 507, 516, and 522 nm for the cases of 2.1, 2.0, and 1.9 mL of (Se+S)-TOP, respectively (Figure 1b), were slightly blue-shifted by 2−3 nm compared to those of CdSe@ZnS ones. These blue-shifts directly result from the band gap widening as recognized from the comparison of absorption spectra (Figure 1Sa, Supporting Information), being attributable to the interfacial alloying throughout the shelling reaction. As shown in PL spectral comparison (Figure 1Sb, Supporting Information), the better surface passivation afforded by such an additional shelling led to about 2 fold-increase in PL QY of 79−83%. Also the emission bandwidths (21 nm) of CdSe@ZnS/ZnS QDs became a little narrower as compared to those (23 nm) of their CdSe@ZnS counterparts. In multicompositional QD systems such as the present quaternary Cd−Zn−Se−S QDs, both chemical composition and size of the QDs jointly determine the band gap energy (or emission wavelength), and their dispersion degrees directly influence the emission bandwidth. Assuming that the actual core sizes in CdSe@ZnS QDs would remain invariant after an additional shelling, the emission narrowing observed (Figure 1b) is presumably ascribable to the compositional homogenizing assisted by the aforementioned interfacial alloying. The representative 516 nm-emitting CdSe@ZnS/ZnS QD sample prepared with 2.0 mL of (Se+S)-TOP, exhibiting a strong fluorescence under UV irradiation, is shown in Figure 1d.

In most of visible-emitting core/shell QDs, ZnS is the most commonly chosen shell composition, since its sufficiently high band gap provides large electron/hole band offset potentials in the form of type I electronic structure. Except for our recently developed blue CdZnS/ZnS QDs[8] the sizes of such heterostructured QDs reported to date are below 10 nm irrespective of their visible emission wavelengths, indicative of the synthetic difficulty of larger-sized QDs with thicker ZnS shells. Although giant-shell CdSe/CdS QDs with ultrashell thickness up to 16 MLs were proposed as promising alternatives to the conventional thin-shell counterparts for minimizing the photoblinking *via* an AR suppression,[28,29] the compositional combination of these giant-structured QDs has been confined to the CdSe core/CdS shell only, since they show a minimal lattice mismatch required for a thick shell growth. Unfortunately, these excessively thick-shell QDs exhibited only moderate QY values due to the generation of more internal defects with increasing CdS shell.[29] And such a given compositional system of CdSe/CdS provides a quasi-type II electronic structure, where a hole is strongly confined into core, while an electron is extensively delocalized into shell, lowering the confinement energy and consequent excitonic transition energy. Hence, the emission wavelength of giant-shell CdSe/CdS QDs has been tailored mainly by varying CdS shell thickness with the size of CdSe core almost fixed, but the resulting spectral tunability was quite narrow within a primary window of red emission.[20,28,29] The average size of our CdSe@ZnS QDs was estimated to be 9.5 nm based on high-resolution transmission electron microscopic (TEM) image (Figure 2a). And CdSe@ZnS/ZnS QDs obtained through the consecutive ZnS shelling possessed a bigger size of 12.7 nm by an additional overgrowth of 1.6 nm-thick ZnS (corresponding to ~5.2 MLs) (Figure 2b). This size difference could also be readily noticed from low-magnification TEM images (Figure S2, Supporting Information). If it is consdiered that the gradient-shell composition of CdSe@ZnS

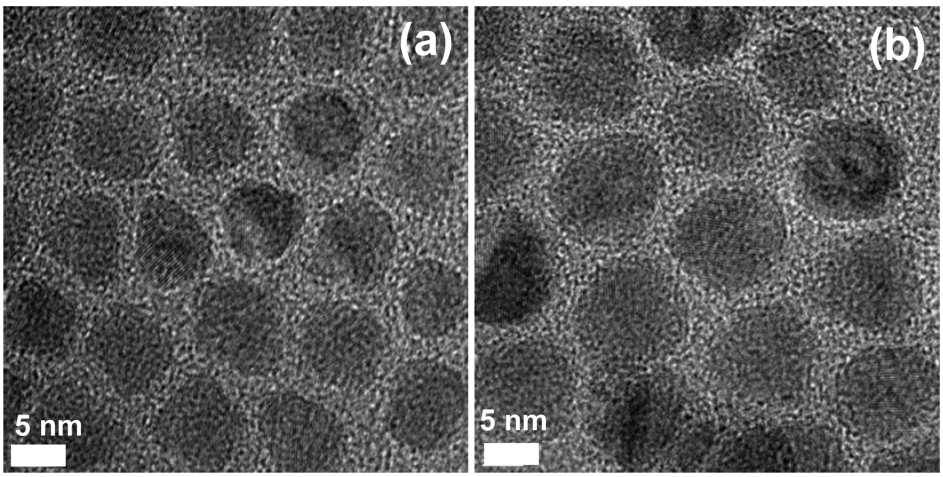

Figure 2. High-resolution TEM images of (a) CdSe@ZnS and (b) CdSe@ZnS/ZnS QDs with the average sizes of 9.5 and 12.7 nm, respectively (scale bar, 5 nm).

QDs would consist of gradually increasing Zn and S contents with a QD radius and finally a pure ZnS outward, the actual thickness of ZnS shell in CdSe@ZnS/ZnS QDs should be thicker than 1.6 nm. It is worth noting that the present CdSe@ZnS/ZnS QDs are the largest ones as compared with ZnS-shelled R, G, and B QDs reported previously.

An initial strong PL of as-prepared QDs is usually not retained after a thorough purification cycle, typically attributable to the gradual physical detachment of surface capping ligands with the repetition number of purification. To address this QY reduction concomitant to the purification step, the replacement of labile TOP ligand with more strongly binding thiol[13] or oleate species[8,18] and the structural improvement of core/shell QDs with multishell[6,30] or giant-shell[29] have been effectively attempted. Figure S3a (Supporting Information) presents the comparison of PL QY variations of 2.0 mL (Se+S)-TOP-based QDs without *versus* with an additional ZnS shell against a purification cycle with the repeated round up to 8 times. CdSe@ZnS QDs suffered from an archetypal QY deterioration as the purification was repeated. The QY of 8×-purified QD sample reached only 24%, corresponding to a 43% drop relative to the original QY. In contrast, CdSe@ZnS/ZnS QDs displayed an excellent fluorescent stability, retaining the initial high QY (83%) even after an 8×-purification cycle. A sufficiently thick ZnS shell may serve as an effective physical barrier in preventing the electron/hole wave functions of core domain from leaking into QD surface trap sites, rendering the excitonic recombination immune to the undesirable change of QD surface environment (*e.g.*, ligand loss). A hydrophobic-to-hydrophilic ligand exchange of QDs is a common process to obtain water-soluble QDs required for biological applications. In general, PL of ligand-exchanged QDs is markedly quenched, usually attributable to the creation of nonradiative trap sites by the ligand exchange-involved devastation of QD surface. Hydrophobic surface ligands of CdSe@ZnS/ZnS QDs were readily exchanged with a hydrophilic mercaptopropionic acid (MPA) (see the Supporting Information for a detailed ligand-exchange procedure). In contrast to the previous results on PL reduction of ligand-exchanged QDs,[30,31] PL intensity of MPA-capped CdSe@ZnS/ZnS QDs well maintained that of its hydrophobic counterparts (Figure S3b, Supporting Information), again supporting that the presence of thick ZnS shell enables QDs to possess a high fluorescent stability against the environmental change of QD surface.

Although core/shell structured QDs usually possess excellent QYs in solution state, their QYs in the form of closely packed thin film become severely reduced as a result of the efficient nonradiative FRET, typically retaining <20%.[14,32,33] Since the rate of FRET (R_{FRET}) is sensitively dependent on inter-QD spacing (d) with the relation of $R_{FRET} \sim d^{-6}$,[34] the degree of this self-quenching can be dictated by QD ligand length and/or shell thickness. Hence, the QDs with longer hydrocarbon chain ligand and/or thicker shell would be highly advantageous in suppressing the FRET and thereby achieving the high device efficiency of QLED comprising thin film QD EML. Figure 3a shows the comparison of QYs of CdSe@ZnS and CdSe@ZnS/ZnS QDs in solution *versus* film states. The QY (18%) of ~30 nm-thick CdSe@ZnS QD film was appreciably reduced by about 57% compared to the solution value, indicative of a high degree of FRET. In the case of CdSe@ZnS/ZnS QDs, however, the QY deviation between solution (83%) *versus* ~40 nm thick film (inset of Figure 3a) (71%) was much smaller, directly resulting from the effectively lowered FRET efficiency enabled by the additional 1.6 nm thick physical barrier of ZnS shell. PL lifetimes of QD exciton emissions in solution *versus* film states were also assessed to further support the results in Figure 3a. The lifetime of QDs in solution is naturally reduced when they are transferred to a solid film, attributable to the involvement of nonradiative

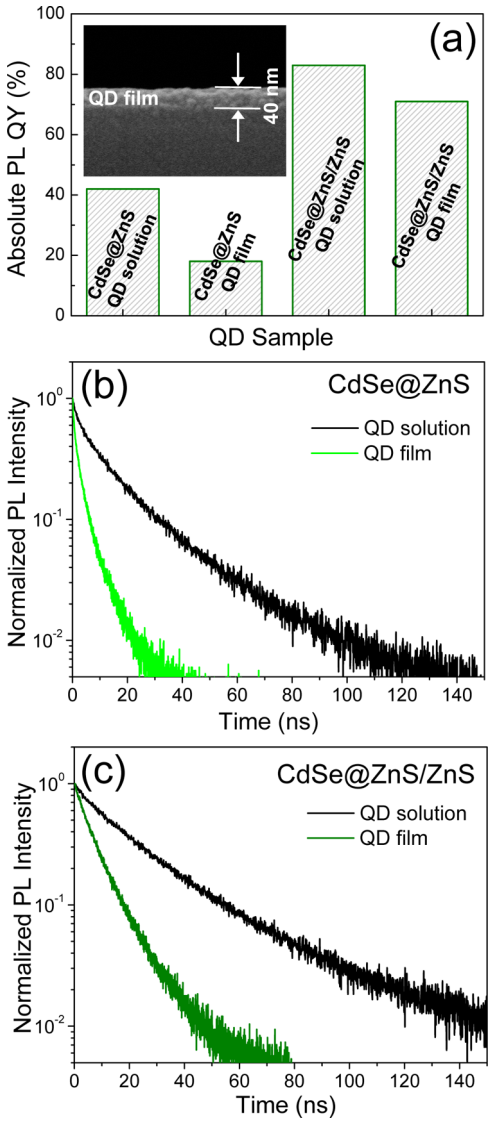

Figure 3. (a) Comparison of PL QYs of CdSe@ZnS and CdSe@ZnS/ZnS QDs in the forms of solution *versus* solid film. Variations of PL lifetime in solution *versus* film states of (b) CdSe@ZnS and (c) CdSe@ZnS/ZnS QDs. The thicknesses of film samples were ~30 and ~40 nm (inset of (a)) for the former and latter QDs, respectively.

processes such as FRET and/or the exposure of dipole to an inhomogeneous environment (*e.g.*, substrate/QD/air) instead of a homogeneous one for the case of QD solution.[35] CdSe@ZnS QDs showed a single exciton lifetime of 21.4 ns in solution, in line with the values (20−30 ns) reported from relatively thin-shell QDs,[36,37] but a drastic lifetime shortening to 4.9 ns was observed in their ~30 nm-thick film sample (Figure 3b). Meanwhile, as compared with CdSe@ZnS QDs, CdSe@ZnS/ZnS QDs showed a little longer solution PL lifetime of 27.2 ns (Figure 3c). This slower PL decay may be correlated to the decreased contribution of nonradiative process in the exciton decay, also consistent with their improved QY. The decay time of CdSe@ZnS/ZnS QDs was also shortened to 9.2 ns for ~40 nm-thick film sample. But this shortening (~34%) is less pronounced

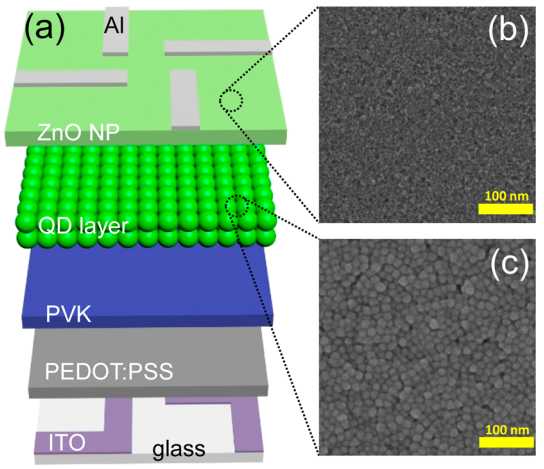

Figure 4. (a) Schematic illustration of all-solution-processed, multilayered green QLED consisting of ITO//PEDOT:PSS//PVK//CdSe@ZnS or CdSe@ZnS/ZnS QDs//ZnO NPs//Al. Surface SEM images of uniformly, compactly packed (b) ETL of ZnO NPs and (c) EML of CdSe@ZnS/ZnS QDs.

compared to that (~23%) observed in CdSe@ZnS QD case. Furthermore, the decay times of CdSe@ZnS/ZnS QD film sample at spectrally distinct positions of 497, 516, and 535 nm were collected (Figure S4, Supporting Information), showing only moderate reduction from 10.8 to 8.1 ns with increasing emission energy. These PL decay results can further support that the additional ZnS shell layer in CdSe@ZnS/ZnS QDs served as an effective spacer in reducing the FRET probability between interacting QD dipoles.

CdSe@ZnS *versus* CdSe@ZnS/ZnS QDs-based green QLEDs were constructed with the conventional device scheme *via* all-solution processing of the constituent layers except for Al cathode (Figure 4a), largely following the fabrication procedures of our recent blue QLED[8] with some processing modifications for the optimization of EML and ETL thicknesses. In brief, the coating solutions of poly(ethylenedioxythiophene):polystyrenesulfonate (PEDOT:PSS), PVK dissolved in chlorobenzene, CdSe@ZnS or CdSe@ZnS/ZnS QDs dispersed in hexane, and ZnO NPs (see the Supporting Information for synthetic details) dispersed in ethanol were sequentially spin-deposited onto a patterned ITO glass. The device fabrication was completed by thermal evaporation of Al, consisting of multilayered structure of 160 nm thick ITO//20 nm thick PEDOT:PSS//20 nm thick PVK//30 nm thick CdSe@ZnS or 40 nm thick CdSe@ZnS/ZnS QDs (corresponding to about 3 MLs of QDs for both cases)//50 nm-thick ZnO NPs//100 nm-thick Al (Figure S5a−c, Supporting Information) with four 3 × 3 mm^2 square-shaped emitting spots. Since the hexane that disperses QDs does not dissolve PVK, the spin-coating of the QD−hexane dispersion neither damaged the underlying PVK HTL nor caused an interlayer mixing. Relatively uniform surface morphologies of spin-deposited, compactly packed QD and ZnO NP layers are also seen from scanning electron microscopic (SEM) images of Figure 4b,c, respectively.

Figure 5a shows the variations of current density and luminance with a voltage sweep to 11 V for two green QLEDs integrated with 518 nm-emitting CdSe@ZnS *versus* 516 nm-emitting CdSe@ZnS/ZnS QDs. The peak luminances of 9010 (at 9.5 V) and 85700 cd/m^2 (at 9 V) from CdSe@ZnS and CdSe@ZnS/ZnS QLEDs, respectively, were achieved. The current densities of CdSe@ZnS/ZnS QLED were substantially lower than those of the CdSe@ZnS QLED throughout the entire bias range, for instance, 322 and 413 mA/cm^2 at 9 V from the former and latter devices, respectively, being ascribable to the combined effect of the following points. First, the thickness of QD EML was different for those two QLEDs (as specified above), indicative of a lower effective electric field and consequently a lower charge injection from CdSe@ZnS/ZnS *versus* CdSe@ZnS QLED. Second, the charge injection into the QD EML region from respective CTLs could be more impeded in CdSe@ZnS/ZnS QLED compared to its CdSe@ZnS QD counterpart by means of the presence of a thicker ZnS shell as a nontrivial energetic barrier against the charge injection. As a direct consequence of lower leakage currents along with higher luminances, CdSe@ZnS/ZnS QLED overwhelmingly outperformed CdSe@ZnS one with respect to device efficiency. The peak CE and EQE of CdSe@ZnS QLED reached 2.1 cd/A and 0.5%, respectively, while an additional 1.6 nm thick ZnS shell gave rise to the drastic improvement in device efficiency of the peak values of CE of 46.4 cd/A and EQE of 12.6% (Figure 5b and Figure S6a,b, Supporting Information). These exceptional peak efficiencies of our green CdSe@ZnS/ZnS QLED were more than as high as compared to the highest efficiency values of CE of 19.2 cd/A and EQE of 5.8% reported to date from a partially solution-processed, inverted structure green (520 nm) QLED.[18] Note here that these peak efficiencies were not record values but rather medium ones obtained among six devices of CdSe@ZnS/ZnS QLED tested, as shown in the distributions of EQE and CE (Figure S7, Supporting Information). The efficiency roll-off behavior was observed at high driving bias or current regimes, typically attributable to the electric field-induced increasing spatial separation of electron/hole wave functions (leading to the reduced radiative recombination rate)[32] and/or the increasing degree of QD charging (leading to the increased nonradiative Auger decay rate).[21] It is also noted that the CE and PE of CdSe@ZnS/ZnS QLED were approximated to be as high as ~45 cd/A and ~19 lm/W, respectively, even at a high luminance level of 10000 cd/m^2 (Figure S8, Supporting Information).

Compared to the ~4-fold increase in film QY of CdSe@ZnS/ZnS *versus* CdSe@ZnS QDs, ~25-fold increase in EQE of CdSe@ZnS/ZnS *versus* CdSe@ZnS QLEDs implies that the device efficiency should be determined more critically by the efficiency of radiative exciton formation in QD EML of device than QY.

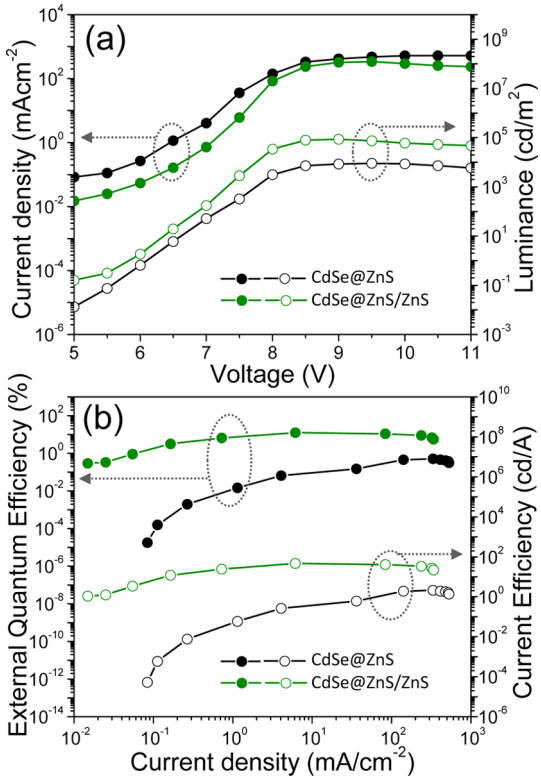

Figure 5. Variations of (a) current density and luminance with increasing applied voltage and (b) EQE and CE as a function of current density for CdSe@ZnS *versus* CdSe@ZnS/ZnS QLEDs.

Current density-dependent variations of EQE and CE (Figure 5b) indicate that under the same current flow the radiative recombination of electrically excited QDs occurs much more efficiently in CdSe@ZnS/ZnS QLED *versus* CdSe@ZnS one. Two main factors of FRET and QD charging-related AR processes are likely involved in determining the QD luminescence efficiency of device. The beneficial role of a thicker ZnS shell of CdSe@ZnS/ZnS QDs in suppressing inter-QD FRET event, which was seen from the retention of high PL QY even in solid-state film and supported by the analysis of PL dynamics (Figure 3 and Figure S4, Supporting Information), should be also valid in QD EML of device, being directly but partly responsible for the observed drastic improvements in luminance and efficiencies. The relative energetic positions of highest occupied molecular orbital (HOMO) and lowest unoccupied molecular orbital (LUMO) of QD EML *versus* the neighboring CTLs are of critical importance in facilitating a charge injection and balancing the injected charges. In the case of hybrid QLEDs consisting organic HTL plus inorganic ETL, a considerable hole injection barrier at HTL/QD interface exists owing to the intrinsically deep-lying HOMO level of QD, whereas an energy barrier-free electron injection occurs due to the similarly aligned energy levels at QD/ETL interface, as suggested in the schematic energy diagram of our hybrid QLED (Figure S5d, Supporting Information). These asymmetric

barriers render the electron injection to QD EML dominant, inevitably leading to the QD charging induced by the unbalanced injected charge carriers. Then, the QDs charged with excess electrons become situated under a very efficient multicarrier AR process, readily losing their emissivity.[20] In the case of giant-shell CdSe/CdS QDs, the AR process has become more suppressed with increasing CdS shell thickness as a result of a more delocalization of electron and consequently more reduction of the overlap of electron/hole wave functions in such a quasi-type II system.[21,36] Meanwhile, in our QDs with a type I electronic structure, both charge carriers would be localized into core domain, and thus the effective volume of exciton involved with AR process would remain largely independent of ZnS shell thickness. This consideration leads to the conclusion that the presence of a thicker ZnS shell itself little contribute to the reduction of AR process at the charged QDs. The insertion of alloyed layer at core/shell interface, typically forming CdSe/CdSeS/CdS structure, has been attempted and found to be an even more powerful strategy for AR suppression as comparison to the growth of a thick CdS shell.[21,24,36] The alloyed layer affords a smoothing of core/shell interfacial potential, thereby decreasing the wave function overlap of the initial and final states of the carrier excited during the course of Auger decay.[21] Such an interfacial alloyed layer is expected to be naturally formed in both QDs of CdSe@ZnS and CdSe@ZnS/ZnS, which consist of intermediate CdSe-ZnS alloyed shells with the composition gradient in a radial direction plus outer ZnS shells, as described earlier. The beneficial effect of the alloyed layer on AR suppression is likely more appreciable in CdSe@ZnS/ZnS *versus* CdSe@ZnS QDs, since the additional ZnS overgrowth of the former QDs would make the alloyed layer positioned in a more inner side compared to the latter ones, affording a more solid, complete structure of core/alloyed shell/outer shell and ultimately improving the device efficiency.

A gradual EL shift to lower energy with increasing voltage is general in most of QLEDs, attributable to a field-induced quantum confinement Stark effect (QCSE),[16,33] and EL bandwidth is also field-dependent, becoming broader with higher voltages. This spectral broadening may be caused by an increased LO (longitudinal optical)-phonon interaction accompanied by a large degree of exciton polarization by high electric field.[16] Such spectral instabilities, leading to a lack of color reproducibility, with driving voltage should be avoided for the practical application of QLED to high-quality display. Figure 6a presents the voltage-dependent evolution of normalized EL spectra of CdSe@ZnS/ZnS QLED. The EL spectra collected at applied voltages up to 9 V (corresponding to 322 mA/cm^2) remained largely unchanged with the identical peak wavelength (516 nm) and bandwidth (21 nm), also

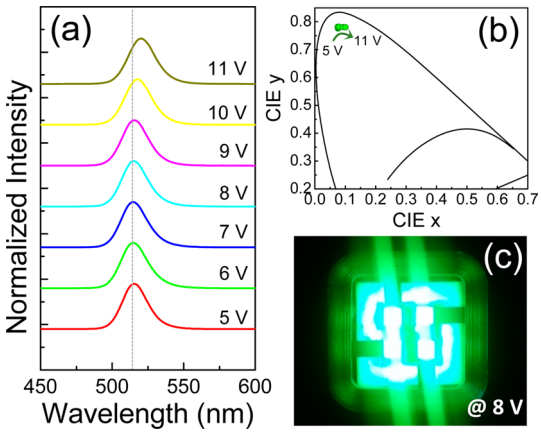

Figure 6. Comparison of (a) normalized EL spectra and (b) corresponding CIE color coordinates from CdSe@ZnS/ZnS QLED with increasing applied voltage up to 11 V. (c) Photographic image showing highly bright EL emission from four emitting spots at a driving voltage of 8 V.

coinciding with solution PL results (Figure 1b) of CdSe@ZnS/ZnS QDs. Hence, the resulting Commission Internationale de l'Eclairage (CIE) color coordinates were only slightly varied in the narrow range of (0.075−0.079, 0.776−0.782) under applied voltages of 5−9 V (Figure 6b). Thanks to an extremely narrow emission together with a well-adjusted emission wavelength, EL was appropriately positioned in a deep corner of green region in the color space, producing an exceptionally pure green EL that should contribute to a substantially widened color gamut of display. A highly bright, color-saturated green EL image collected from CdSe@ZnS/ZnS QLED during the operation at 8 V is also shown in Figure 6c. The unusual observation of this persistent EL spectral retention even under such a high voltage suggests that CdSe@ZnS/ZnS QDs may be resistant to the field-induced exciton polarization due to the presence of thick ZnS shell. This thick shell presumably functions as a physical spacer that may screen the external field, effectively impeding the exciton polarization.[8] Upon application of higher voltage of 10 V, however, EL began to be slightly red-shifted to 518 nm, adjunctively accompanied by a little broadened bandwidth of 22 nm. Such EL spectral alterations became more pronounced at 11 V, showing a peak wavelength of 520 nm, bandwidth of 23 nm, and somewhat deviated color coordinates of (0.101, 0.781), presumably due to the eventual appearance of exciton polarization only under excessively strong electric fields.

CONCLUSION

The successful overgrowth of an additional ZnS outer shell onto 9.5 nm-sized, composition gradient-shell CdSe@ZnS QDs, resulting in extraordinarily large-sized (12.7 nm) CdSe@ZnS/ZnS QDs, was demonstrated. While PL QY of a solid film of CdSe@ZnS QDs was significantly reduced compared to that of their

solution sample, CdSe@ZnS/ZnS QDs exhibited a much lower QY deviation of 83 *versus* 71% for solution *versus* solid film, respectively, which was attributable to the effectively lowered FRET efficiency enabled by the additionally overgrown ZnS shell, and also supported by PL lifetime analysis. Two multilayered hybrid green QLEDs containing CdSe@ZnS *versus* CdSe@ZnS/ZnS have been identically fabricated by a sequential solution-processing, and their EL performances were compared. While the peak CE and EQE of CdSe@ZnS QLED reached only 2.1 cd/A and 0.5%, respectively, an additional 1.6 nm thick ZnS shelling led to the drastically improved device efficiency of the peak values of CE of 46.4 cd/A and EQE of 12.6%. These exceptional efficiencies, which are at least 2-fold higher as compared to the highest values of CE of 19.2 cd/A and EQE of 5.8% reported to date, were believed to be attributable to the benefit of our unique QD structure, where nonradiative processes of inter-QD FRET and QD charging-accompanying AR are effectively suppressed. Therefore, our study clearly suggests how critical the structural QD engineering is in determining QLED efficiency. No spectral diffusion of EL of CdSe@ZnS/ZnS QLED against the voltage variation up to 9 V was also observed and explained with the role of thick ZnS shell.

EXPERIMENTAL SECTION

Synthesis of Green CdSe@ZnS and CdSe@ZnS/ZnS QDs. In a single-step synthesis of composition gradient-shell CdSe@ZnS QDs, 0.14 mmol of Cd acetate and 3.41 mmol of Zn oxide were mixed with 7 mL of OA in 50 mL of three-neck flask. This mixture was heated to 150 °C simultaneously with Ar purging. Then, 15 mL of 1-octadecene (ODE) was added into the reactor at that temperature, and the whole mixture was further heated to 310 °C. Separately, an anionic stock solution was prepared by dissolving 5 mmol of Se and 5 mmol of S in 5 mL of TOP. Then, 1.9, 2.0, or 2.1 mL of (Se+S)-TOP was swiftly injected into the above hot mixture and the reaction proceeded at that temperature for 10 min for the growth of CdSe@ZnS QDs. For producing uniquely large-sized CdSe@ZnS/ZnS QDs through an additional ZnS overcoating, 1.6 mmol of S dissolved in 2.4 mL of ODE was consecutively introduced into the above growth solution of CdSe@ZnS QDs at the same temperature, followed by a holding time of 12 min. Next, a Zn stock solution, prepared by 2.86 mmol of Zn acetate dehydrate dissolved in a mixture of 1 mL of OA and 4 mL of ODE, was injected at 310 °C, after which the temperature of reaction became lowered to 270 °C. Then, an S stock solution, prepared by 9.65 mmol of S dissolved in 5 mL of TOP, was dropwisely introduced in a rate of ~0.5 mL/min, and the additional ZnS shelling proceeded at that temperature for 20 min. The resulting CdSe@ZnS and CdSe@ZnS/ZnS QDs were precipitated by adding excess ethanol and repeatedly washed with a solvent combination of hexane/ethanol (1:4 in volume ratio) by centrifugation (12000 rpm, 10 min), and the purified QDs were redispersed in chloroform for optical characterizations and ligand exchange and hexane for spin-deposition of solid-state QD layers.

Fabrication Procedures of Multilayered Green QLEDs. A patterned ITO glass substrate was thoroughly cleaned sequentially with DI water, acetone, and 2-propanol for 15 min each and then treated with UV-ozone for 20 min. PEDOT:PSS (AI 4083) (~20 nm thick) as a HIL was spin-deposited at 3000 rpm for 60 s, followed by baking at 150 °C for 30 min in a N_2-purged glovebox. With a solution of 0.05 g PVK (average M_W = 25000−50000) dissolved in 5 mL of chlorobenzene ~20 nm-thick HTL was formed on top of HIL and baked with the same spinning/baking conditions as in the above HIL. With two QD hexane dispersions of CdSe@ZnS and CdSe@ZnS/ZnS having an identical optical density (OD) of ~3.0 at the respective excitonic absorption peaks, corresponding to about 9 and 15 mg/mL, respectively, QD EMLs with about 3 MLs were spin-deposited at 2000 rpm for 20 s and subsequently dried at room temperature. An optically transparent ethanol solution dispersed with ZnO NPs, having a concentration of ~30 mg/mL, was again spin-coated at 1500 rpm for 60 s, followed by the baking (60 °C for 30 min). The multilayered device fabrication was completed by a thermally evaporated 100 nm-thick Al cathode.

Conflict of Interest: The authors declare no competing financial interest.

Acknowledgment. This work was supported by the National Research Foundation of Korea (NRF) grant funded by the Korea government (MSIP) (No. 2013R1A2A2A01068158) and by the Converging Research Center Program through the Ministry of Science, ICT and Future Planning, Korea (2013K000182). It was also supported in part by Samsung Display Co., Ltd.

Supporting Information Available: Synthesis of ZnO NPs, hydrophobic-to-hydrophilic ligand exchange processing of QDs, material/device characterization, absorption/PL spectra, and low-magnification TEM images, variations of solution PL QY with a repeated number of purification of CdSe@ZnS *versus* CdSe@ZnS/ZnS QDs, spectral comparison of original hydrophobic *versus* MPA-capped hydrophilic CdSe@ZnS/ZnS QDs, cross-sectional SEM images and proposed energy levels of multilayered device with CdSe@ZnS/ZnS QDs, and variations of EQE/CE with increasing applied voltage and CE/PE as a function of luminance for CdSe@ZnS *versus* CdSe@ZnS/ZnS QLEDs. This material is available free of charge *via* the Internet at http://pubs.acs.org.

REFERENCES AND NOTES

1. Stouwdam, J. W.; Janssen, R. A. J. Red, Green, and Blue Quantum Dot LEDs with Solution Processable ZnO Nanocrystal Electron Injection Layers. *J. Mater. Chem.* **2008**, *18*, 1889–1894.
2. Cho, K. S.; Lee, E. K.; Joo, W. J.; Jang, E.; Kim, T. H.; Lee, S. J.; Kwon, S. J.; Han, J. Y.; Kim, B. K.; Choi, B. L.; et al. High-Performance Crosslinked Colloidal Quantum-Dot Light-Emitting Diodes. *Nat. Photonics* **2009**, *3*, 341–345.
3. Kim, T. H.; Cho, K. S.; Lee, E. K.; Lee, S. J.; Chae, J.; Kim, J. W.; Kim, D. H.; Kwon, J. Y.; Amaratunga, G.; Lee, S. Y.; et al. Full-Colour Quantum Dot Displays Fabricated by Transfer Printing. *Nat. Photonics* **2011**, *5*, 176–182.
4. Qian, L.; Zheng, Y.; Xue, J. G.; Holloway, P. H. Stable and Efficient Quantum-Dot Light-Emitting Diodes Based on Solution-Processed Multilayer Structures. *Nat. Photonics* **2011**, *5*, 543–548.
5. Shen, H. B.; Wang, S.; Wang, H. Z.; Niu, J. Z.; Qian, L.; Yang, Y. X.; Titov, A.; Hyvonen, J.; Zheng, Y.; Li, L. S. Highly Efficient Blue-Green Quantum Dot Light-Emitting Diodes Using Stable Low-Cadmium Quaternary-Alloy ZnCdSSe/ZnS Core/Shell Nanocrystals. *ACS Appl. Mater. Interfaces* **2013**, *5*, 4260–4265.
6. Shen, H. B.; Lin, Q. L.; Wang, H. Z.; Qian, L.; Yang, Y. X.; Titov, A.; Hyvonen, J.; Zheng, Y.; Li, L. S. Efficient and Bright Colloidal Quantum Dot Light-Emitting Diodes *via* Controlling the Shell Thickness of Quantum Dots. *ACS Appl. Mater. Interfaces* **2013**, *5*, 12011–12016.
7. Leck, K. S.; Divayana, Y.; Zhao, D. W.; Yang, X. Y.; Abiyasa, A. P.; Mutlugun, E.; Gao, Y.; Liu, S. W.; Tan, S. T.; Sun, X. W.; et al. Quantum Dot Light-Emitting Diode with Quantum Dots Inside the Hole Transporting Layers. *ACS Appl. Mater. Interfaces* **2013**, *5*, 6535–6540.

8. Lee, K. H.; Lee, J. H.; Song, W. S.; Ko, H.; Lee, C.; Lee, J. H.; Yang, H. Highly Efficient, Color-Pure, Color-Stable Blue Quantum Dot Light-Emitting Devices. *ACS Nano* **2013**, *7*, 7295–7302.
9. Shirasaki, Y.; Supran, G. J.; Bawendi, M. G.; Bulovic, V. Emergence of Colloidal Quantum-Dot Light-Emitting Technologies. *Nat. Photonics* **2013**, *7*, 13–23.
10. Zhao, J. L.; Bardecker, J. A.; Munro, A. M.; Liu, M. S.; Niu, Y. H.; Ding, I. K.; Luo, J. D.; Chen, B. Q.; Jen, A. K. Y.; Ginger, D. S. Efficient CdSe/CdS Quantum Dot Light-Emitting Diodes Using a Thermally Polymerized Hole Transport Layer. *Nano Lett.* **2006**, *6*, 463–467.
11. Anikeeva, P. O.; Halpert, J. E.; Bawendi, M. G.; Bulovic, V. Electroluminescence from a Mixed Red-Green-Blue Colloidal Quantum Dot Monolayer. *Nano Lett.* **2007**, *7*, 2196–2200.
12. Sun, Q.; Wang, Y. A.; Li, L. S.; Wang, D. Y.; Zhu, T.; Xu, J.; Yang, C. H.; Li, Y. F. Bright, Multicoloured Light-Emitting Diodes Based on Quantum Dots. *Nat. Photonics* **2007**, *1*, 717–722.
13. Bae, W. K.; Kwak, J.; Park, J. W.; Char, K.; Lee, C.; Lee, S. Highly Efficient Green-Light-Emitting Diodes Based on CdSe@ZnS Quantum Dots with a Chemical-Composition Gradient. *Adv. Mater.* **2009**, *21*, 1690–1694.
14. Anikeeva, P. O.; Halpert, J. E.; Bawendi, M. G.; Bulovic, V. Quantum Dot Light-Emitting Devices with Electroluminescence Tunable over the Entire Visible Spectrum. *Nano Lett.* **2009**, *9*, 2532–2534.
15. Wood, V.; Panzer, M. J.; Halpert, J. E.; Caruge, J. M.; Bawendi, M. G.; Bulovic, V. Selection of Metal Oxide Charge Transport Layers for Colloidal Quantum Dot LEDs. *ACS Nano* **2009**, *3*, 3581–3586.
16. Wood, V.; Panzer, M. J.; Caruge, J. M.; Halpert, J. E.; Bawendi, M. G.; Bulovic, V. Air-Stable Operation of Transparent, Colloidal Quantum Dot Based LEDs with a Unipolar Device Architecture. *Nano Lett.* **2010**, *10*, 24–29.
17. Bae, W. K.; Kwak, J.; Lim, J.; Lee, D.; Nam, M. K.; Char, K.; Lee, C.; Lee, S. Multicolored Light-Emitting Diodes Based on All-Quantum-Dot Multilayer Films Using Layer-by-Layer Assembly Method. *Nano Lett.* **2010**, *10*, 2368–2373.
18. Kwak, J.; Bae, W. K.; Lee, D.; Park, I.; Lim, J.; Park, M.; Cho, H.; Woo, H.; Yoon, D. Y.; Char, K.; et al. Bright and Efficient Full-Color Colloidal Quantum Dot Light-Emitting Diodes Using an Inverted Device Structure. *Nano Lett.* **2012**, *12*, 2362–2366.
19. Mashford, B. S.; Stevenson, M.; Popovic, Z.; Hamilton, C.; Zhou, Z. Q.; Breen, C.; Steckel, J.; Bulovic, V.; Bawendi, M.; Coe-Sullivan, S.; et al. High-Efficiency Quantum-Dot Light-Emitting Devices with Enhanced Charge Injection. *Nat. Photonics* **2013**, *7*, 407–412.
20. Pal, B. N.; Ghosh, Y.; Brovelli, S.; Laocharoensuk, R.; Klimov, V. I.; Hollingsworth, J. A.; Htoon, H. 'Giant' CdSe/CdS Core/Shell Nanocrystal Quantum Dots As Efficient Electroluminescent Materials: Strong Influence of Shell Thickness on Light-Emitting Diode Performance. *Nano Lett.* **2012**, *12*, 331–336.
21. Bae, W. K.; Park, Y. S.; Lim, J.; Lee, D.; Padilha, L. A.; McDaniel, H.; Robel, I.; Lee, C.; Pietryga, J. M.; Klimov, V. I. Controlling the Influence of Auger Recombination on the Performance of Quantum-Dot Light-Emitting Diodes. *Nat. Commun.* **2013**, *4*, 2661.
22. Lim, J.; Park, M.; Bae, W. K.; Lee, D.; Lee, S.; Lee, C.; Char, K. Highly Efficient Cadmium-Free Quantum Dot Light-Emitting Diodes Enabled by the Direct Formation of Excitons within InP@ZnSeS Quantum Dots. *ACS Nano* **2013**, *7*, 9019–9026.
23. Wang, X. Y.; Ren, X. F.; Kahen, K.; Hahn, M. A.; Rajeswaran, M.; Maccagnano-Zacher, S.; Silcox, J.; Cragg, G. E.; Efros, A. L.; Krauss, T. D. Non-Blinking Semiconductor Nanocrystals. *Nature* **2009**, *459*, 686–689.
24. Garcia-Santamaria, F.; Brovelli, S.; Viswanatha, R.; Hollingsworth, J. A.; Htoon, H.; Crooker, S. A.; Klimov, V. I. Breakdown of Volume Scaling in Auger Recombination in CdSe/CdS Heteronanocrystals: The Role of the Core-Shell Interface. *Nano Lett.* **2011**, *11*, 687–693.
25. Bae, W. K.; Char, K.; Hur, H.; Lee, S. Single-Step Synthesis of Quantum Dots with Chemical Composition Gradients. *Chem. Mater.* **2008**, *20*, 531–539.
26. Bae, W. K.; Nam, M. K.; Char, K.; Lee, S. Gram-Scale One-Pot Synthesis of Highly Luminescent Blue Emitting $Cd_{1-x}Zn_xS$/ZnS Nanocrystals. *Chem. Mater.* **2008**, *20*, 5307–5313.
27. Song, W. S.; Lee, H. S.; Lee, J. C.; Jang, D. S.; Choi, Y.; Choi, M.; Yang, H. Amine-Derived Synthetic Approach to Color-Tunable InP/ZnS Quantum Dots with High Fluorescent Qualities. *J. Nanopart. Res.* **2013**, *15*, 1750.
28. Mahler, B.; Spinicelli, P.; Buil, S.; Quelin, X.; Hermier, J. P.; Dubertret, B. Towards Non-Blinking Colloidal Quantum Dots. *Nat. Mater.* **2008**, *7*, 659–664.
29. Chen, Y.; Vela, J.; Htoon, H.; Casson, J. L.; Werder, D. J.; Bussian, D. A.; Klimov, V. I.; Hollingsworth, J. A. "Giant" Multishell CdSe Nanocrystal Quantum Dots with Suppressed Blinking. *J. Am. Chem. Soc.* **2008**, *130*, 5026–5027.
30. Lim, J.; Bae, W. K.; Lee, D.; Nam, M. K.; Jung, J.; Lee, C.; Char, K.; Lee, S. InP@ZnSeS, Core@Composition Gradient Shell Quantum Dots with Enhanced Stability. *Chem. Mater.* **2011**, *23*, 4459–4463.
31. Luan, W.; Yang, H.; Wan, Z.; Yuan, B.; Yu, X.; Tu, S. Mercaptopropionic Acid Capped CdSe/ZnS Quantum Dots as Fluorescence Probe for Lead (II). *J. Nanopart. Res.* **2012**, *14*, 762.
32. Bozyigit, D.; Yarema, O.; Wood, V. Origins of Low Quantum Efficiencies in Quantum Dot LEDs. *Adv. Funct. Mater.* **2013**, *23*, 3024–3029.
33. Shirasaki, Y.; Supran, G. J.; Tisdale, W. A.; Bulovic, V. Origin of Efficiency Roll-Off in Colloidal Quantum-Dot Light-Emitting Diodes. *Phys. Rev. Lett.* **2013**, *110*, 217403.
34. Rogach, A. L.; Klar, T. A.; Lupton, J. M.; Meijerink, A.; Feldmann, J. Energy Transfer with Semiconductor Nanocrystals. *J. Mater. Chem.* **2009**, *19*, 1208–1221.
35. Novotny, L.; Hecht, B. *Principles of Nano-Optics*; Cambridge University Press: New York, 2012.
36. Ghosh, Y.; Mangum, B. D.; Casson, J. L.; Williams, D. J.; Htoon, H.; Hollingsworth, J. A. New Insights into the Complexities of Shell Growth and the Strong Influence of Particle Volume in Nonblinking "Giant" Core/Shell Nanocrystal Quantum Dots. *J. Am. Chem. Soc.* **2012**, *134*, 9634–9643.
37. Bae, W. K.; Padilha, L. A.; Park, Y. S.; McDaniel, H.; Robel, I.; Pietryga, J. M.; Klimov, V. I. Controlled Alloying of the Core-Shell Interface in CdSe/CdS Quantum Dots for Suppression of Auger Recombination. *ACS Nano* **2013**, *7*, 3411–3419.